Substitution and Preparation Effects on the Molecular-Scale Morphology of PPV Films

M. Kemerink,*,† J. K. J. van Duren,⊥,† A. J. J. M. van Breemen,‡ J. Wildeman,§ M. M. Wienk,† P. W. M. Blom,§ H. F. M. Schoo,‡ and R. A. J. Janssen†

Eindhoven University of Technology, Group Molecular Materials and Nanosystems, P.O. Box 513, 5600 MB Eindhoven, The Netherlands; TNO Industrial Technology, P.O. Box 6235, 5600 HE Eindhoven, The Netherlands; and Materials Science Centre, University of Groningen, Nijenborgh 4, 9747 AG Groningen, The Netherlands

ABSTRACT: The morphology of spin-cast films of poly(*p*-phenylenevinylene) (PPV) derivatives is studied as a function of the substitution pattern of the conjugated backbone. Moreover, the influence of concentration in the casting solution, annealing, the choice of solvent, and the role of defects are addressed. By using a recently developed scanning-probe technique, we are able to visualize individual polymer chains and aggregates on the surface of spin-cast films. We find that a symmetric substitution pattern strongly promotes interchain aggregation in the surface layer, whereas an unsymmetric pattern in some cases leads to intrachain or self-aggregation. The nature of these intrachain aggregates is further investigated using molecular dynamics simulations. The observed molecular morphologies can in most cases be qualitatively related to macroscopic electrooptical properties. Therefore, our results strongly suggest that the surface morphology may be regarded as indicative of the morphology of the entire film.

Introduction

It is hard to overestimate the current interest in polymer semiconductors. Proven applications of these materials include light-emitting diodes (LEDs),[1−3] field-effect transistors (FETs),[4,5] photovoltaic (PV) cells,[6] photonic devices,[7] and novel memories.[8,9] Because of the vast amount of effort spent on these materials and devices, it has become clear that the functional properties of semiconducting polymers depend critically on what is known as the morphology, i.e., the folding and bending of the polymer molecules and their position and orientation with respect to neighboring chains and/or the substrate.[2] In particular, inter- and intrachain interactions strongly affect virtually all electrical and optical properties of semiconducting polymers in the solid state.[3,10] From an experimental point of view, however, it turned out to be far from trivial to measure the morphology in solid state devices with molecular resolution. Consequently, either spatially averaging techniques were applied[4] or monolayers were studied. The latter are usually not representative for actual devices because of the dominance of polymer−substrate interactions. Alternatively, topographic features in atomic force microscopy (AFM) images were correlated to the molecular morphology, despite the absence of molecular resolution.[11−13] Recently, we were able to obtain molecular resolution on semiconducting polymer films of arbitrary thickness by using dedicated cantilevers in combination with conventional tapping- or intermittent-contact AFM.[14] Here, we apply this technique to systematically investigate the molecular-scale morphology of the extensively studied π-conjugated polymer poly-(*p*-phenylenevinylene) (PPV). In particular, the role of

the substitution pattern and the preparation conditions is investigated. A marked distinction in the tendency to (self-)aggregate is found between symmetrically and unsymmetrically substituted PPVs. Moreover, both postcasting heat treatment and an increasing polymer concentration in the casting solvent are found to increase the (self-)aggregation.

Experimental Section

Materials. In Scheme 1 the structures of the polymers that are used in this work are displayed. Of two substitution patterns, a symmetric and an unsymmetric version are investigated. The unsymmetric polymers of these pairs, poly[2-methoxy-5-(3′,7′-dimethyloctyloxy)-1,4-phenylenevinylene] (MD-MO- or OC$_1$C$_{10}$-PPV) and poly[2-methoxy-5-(2′-ethylhexyloxy)-1,4-phenylenevinylene] (MEH-PPV), are the most widely studied PPV derivatives in the literature. Their symmetric counterparts are poly[2,5-bis(3′,7′-dimethyloctyloxy)-1,4-phenylenevinylene] (BisOC$_{10}$-PPV) and poly[2,5-bis(2′-ethylhexyloxy)-1,4-phenylenevinylene] (BEH- or BisEH-PPV), respectively. Apart from these two pairs, two random copolymers are investigated: the symmetric copolymer of poly[2,5-bis(dodecyloxy)-1,4-phenylenevinylene-*co*-2,5-bis(octadecyloxy)-1,4-phenylenevinylene] (LC-PPV, which shows liquid crystalline behavior) and the unsymmetric random copolymer of 2,5-bis-(chloromethyl)-4-methoxy-1-(3,7-dimethyloctyloxy)benzene and 2,5-bis(chloromethyl)-4′-(3,7-dimethyloctyloxy)-1,1′-biphenyl (PhS-PPV).

Except for the sulfoxy-route PPV, all PPVs were synthesized starting from the corresponding bis(chloromethyl) monomers following a modified Gilch dehydrohalogenation procedure and in situ elimination using an excess base in refluxing 1,4-dioxane.[36] The crude polymers were carefully purified by means of repetitive precipitation to afford PPVs in 55−70% yield. Sulfoxy-route PPVs were synthesized starting from the corresponding sulfoxy monomers following a base-induced polymerization in *sec*-butanol.[37,38] Table 2 gives the M_W and M_N values for the investigated materials, as determined by gel permeation chromatography (GPC). GPC measurements were carried out by high-temperature GPC at 140 °C, using 1,2,4-trichlorobenzene as solvent and narrow MWD polystyrene standard samples as reference.

† Eindhoven University of Technology.
‡ TNO Industrial Technology.
§ University of Groningen.
⊥ Present address: Nanosolar, Inc., 2440 Embarcadero Way, Palo Alto, CA 94303.
* Corresponding author. E-mail: m.kemerink@tue.nl.

Scheme 1. Molecular Structures of the Symmetrically Substituted BisOC$_{10}$-PPV, BisEH (or BEH)-PPV, and the Random Copolymer LC-PPV and the Asymmetrically Substituted MDMO (or OC$_1$C$_{10}$)-PPV, MEH-PPV, and PhS-PPV (for Both Random Copolymers $n = m$)
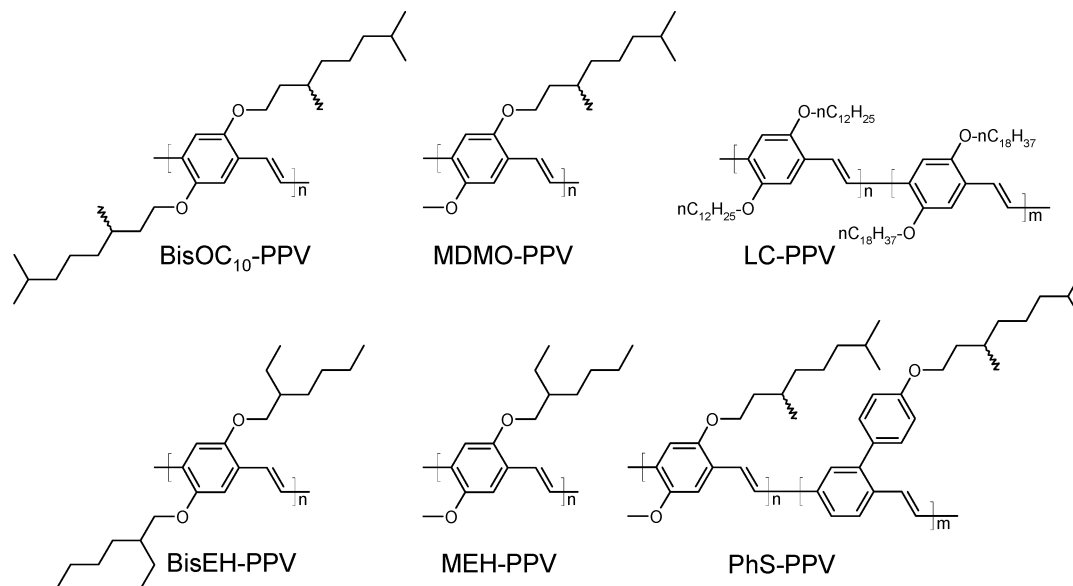
BisOC$_{10}$-PPV   MDMO-PPV   LC-PPV

BisEH-PPV   MEH-PPV   PhS-PPV

Table 1. Zero-Field Hole Mobility μ_0, and Prefactor γ in $\mu(E) = \mu_0 \exp(\gamma\sqrt{E})$ As Measured in LED Geometry and Field-Effect Mobility μ_{FET} As Measured in FET Geometry for the Used Substituted PPVs[a]

structure	μ_0 [cm^2/ (V s)]	γ [(m/V)$^{1/2}$]	μ_{FET} [cm^2/ (V s)]	ref
OC$_1$C$_{10}$-PPV (Gilch)	5×10^{-7}	5.4×10^{-4}	4×10^{-4}	3, 18, 19, 39
OC$_1$C$_{10}$-PPV (sulfoxy)			1×10^{-3}	
MEH-PPV	2×10^{-7}	3.4×10^{-4}	5×10^{-4}	40, 41
PhS-PPV	2×10^{-8}		1×10^{-4}	42, 43
bisOC$_{10}$-PPV	6×10^{-6}	4.0×10^{-4}	1×10^{-3}	3, 18, 19
bisEH-PPV	1×10^{-5}	7.5×10^{-5}	9×10^{-4}	44
LC-PPV	2×10^{-6}		7×10^{-3}	45

[a] For the molecular structures, see Scheme 1.

Table 2. M_W and M_N Values for the Investigated PPVs, As Determined by GPC

structure	M_w [g/mol]	M_n [g/mol]
OC$_1$C$_{10}$-PPV (Gilch)	8.2×10^5	2.3×10^5
OC$_1$C$_{10}$-PPV (sulfoxy)	2.1×10^5	7.4×10^4
MEH-PPV	2.1×10^5	6.3×10^4
bisOC$_{10}$-PPV	7.2×10^5	2.4×10^5
bisEH-PPV	5.5×10^5	1.3×10^5
NRS-PPV	7.5×10^5	2.6×10^5
LC-PPV	1.0×10^6	3.0×10^5

Film Preparation. Fresh solutions were prepared for each set of films. HPLC-grade chlorobenzene is used as solvent, unless indicated otherwise. Prior to spin-casting, the solutions are stirred overnight at room temperature (RT). LC-PPV is prepared at elevated temperatures (solution, substrate, and pipet at 50 °C) to enhance the solubility. The glass substrates are cleaned by rubbing and sonicating with soap (NaSO$_3$C$_{12}$H$_{25}$ in water), followed by washing with water and 2-propanol, and blow-drying with N$_2$. Finally, the substrates are placed in a UV/ozone generator for 20 min. Films were prepared by completely covering the substrate with solution and subsequent spinning at 500 rpm for 7 s, followed by 1500 rpm for 35 s, which yielded ~100 nm thick films for a (default) concentration of 3 mg/mL. An optional annealing step was performed under inert atmosphere by placing the sample on a hot-plate at 100 °C for 20 min, followed by a gradual decrease to 65 °C in 25 min. Further cooling to RT was achieved by placing the samples on a metal plate. Between preparation

and measurement, the films are stored in the dark under inert atmosphere (N$_2$) or vacuum to prevent photooxidation.

Instrumentation. The AFM measurements are performed under ambient conditions on either a Digital Instruments Dimension 3100 with Nanoscope IIIa controller equipped with a home-built phase detection system or a Veeco MultiMode with a Nanoscope IV controller. Metal-coated Si cantilevers (CSC12, NT-MDT with Pt, W or W$_2$C coating) were used in tapping or intermittent-contact mode AFM measurements. All shown measurements are repeated with different scan parameters and on several spots on the same sample to warrant reproducibility and to exclude scan artifacts. Typically, an amplitude set point A/A_0 of 0.7 was used. Special care was taken that sharp, uncontaminated, and comparable tips were used for all samples. Unless stated otherwise, multiple samples, often made on different days, yielded similar results.

FETs were prepared by spin-coating the respective PPVs from chlorobenzene onto OFET test substrates with a bottom contact configuration. Heavily doped silicon was used as the gate electrode, with a HMDS-treated 200 nm thick layer of thermally oxidized SiO$_2$ as the gate-insulating layer. Gold was thermally evaporated and patterned to form interdigitated source and drain contacts. All measurements were performed at 40 °C in air/light using devices with a channel length of 10 mm and a channel width of 20 mm with both gold source and drain bottom electrodes.

Results and Discussion

The main parameters that characterize the electrical behavior of the investigated polymers in LED and FET[16] geometries are given in Table 1. The differences in hole mobility between the symmetrically and unsymmetrically substituted PPVs are much larger than the variance in the values as reported by different laboratories for the same molecular structure. The latter can be mainly attributed to differences in processing conditions and material properties (molecular weight, polydispersity, defects, and purity). So far, no huge differences for the same structure were found as long as the spin-cast solvent was aromatic and resulted in good quality films. Therefore, for our present purposes a comparison as made in Table 1 is allowed. Moreover, it should be noticed that because of the increase of the carrier mobility with charge density, field-effect mobilities μ_{FET} are typically several orders of magnitude larger than those measured in LED configurations.[5]
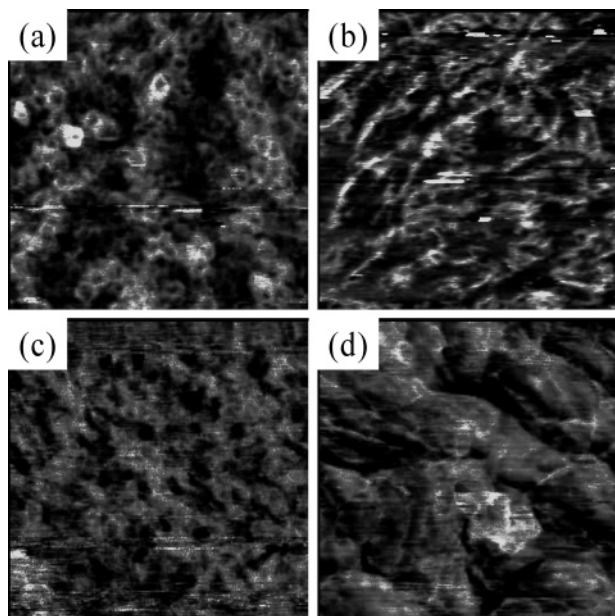
Figure 1. Morphology of (a) OC$_1$C$_{10}$-PPV, (b) BisOC$_{10}$-PPV, (c) MEH-PPV, and (d) BisEH-PPV. Films are pristine and spin-cast from chlorobenzene (3 mg/mL). Scan size 200 × 200 nm.

The Role of Symmetry. The molecular-scale morphology of both pairs of symmetric/unsymmetric PPVs is displayed in Figure 1. The images are obtained as phase signal in normal tapping- or intermittent contact-mode AFM using metal-coated cantilevers with a low spring constant. The observed contrast is caused by the van der Waals interaction between the metal-coated tip and the π-system of the conjugated backbone of the polymer.[14] More details on the AFM measurements can be found in the Experimental Section and in ref 14. The simultaneously obtained topographic images are not displayed as they hardly contain relevant or additional morphological information, unless stated otherwise.[15] Typically, smooth and featureless topographic images are obtained with an rms roughness below 1 nm. Unless heavily aggregated, films of different materials usually cannot be distinguished on the basis of their topography.[14,15]

There is a marked difference between the morphology of OC$_1$C$_{10}$-PPV and BisOC$_{10}$-PPV (see Figure 1a,b). The former shows connected circular features with a typical diameter of 10 ± 2 nm, whereas the latter shows straight features, with a typical length of 20−50 nm. In our previous work we have shown that the observed features are (parts of) molecular chains on the film surface that stand out against the background of the denser packed subsurface layers. In the case of OC$_1$C$_{10}$-PPV these chains have a coiled-up, spiraling conformation or, in the case of BisOC$_{10}$-PPV, have a straight conformation.[14] The coiled-up conformation is illustrated in the insets of Figure 4c. The difference was tentatively attributed to the different symmetry of the substitution pattern. This attribution is strengthened by the observed morphology of MEH- and BisEH-PPV. For MEH-PPV similar, though less well-developed, coiled-up conformations are observed as for OC$_1$C$_{10}$-PPV. By annealing the sample at 100 °C, this conformation develops further and a morphology that is similar to OC$_1$C$_{10}$-PPV is observed. Below, this issue is discussed in a separate subsection. The difference in the degree the circular conformations are developed for pristine films of OC$_1$C$_{10}$- and MEH-PPV is unclear at present
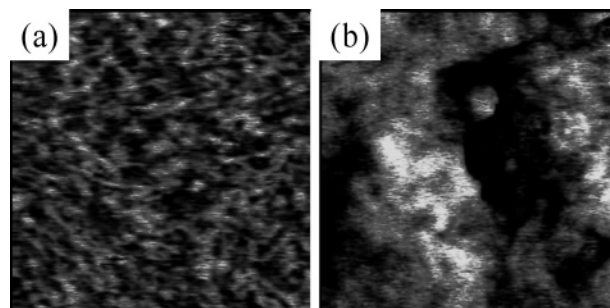

Figure 2. Morphology of (a) PhS-PPV (3 mg/mL) and (b) LC-PPV (0.5 wt %). Films are pristine and spin-cast from chlorobenzene. Scan size 200 × 200 nm.
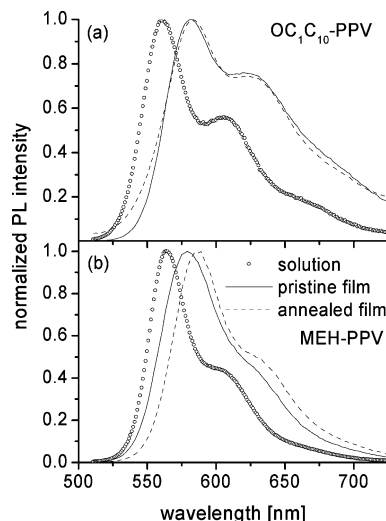

Figure 3. (a) Normalized PL spectra of OC$_1$C$_{10}$-PPV in solution (symbols) and in pristine (solid line) and annealed (dashed line) film. (b) Same for MEH-PPV. Both films are spin-cast from chlorobenzene (2 mg/mL) and annealed at 120 °C.

but is possibly related to differences in defect concentration. The role of defects will be further discussed in the next and in the last subsection. For BisEH-PPV, large ∼50 nm sized relatively homogeneous features are observed. The homogeneity *within* these features indicates a constant response of the sample to the oscillating tip over a large number of chains, which, in this case, implies the delocalization of the electronic ground state over multiple chains.[14] Because of this, and because of their size, the features in Figure 1d are interpreted as aggregates. It is important to point out that these features are extremely similar to the subsurface aggregates that were observed in ref 14 on BisOC$_{10}$-PPV, though the latter are somewhat larger (∼100−200 nm, not shown). The interchain aggregation that is observed in the (sub)surface layer of BisOC$_{10}$- and BisEH-PPV is not observed for their unsymmetric counterparts.

The qualitative difference between the morphologies of symmetrically and unsymmetrically substituted PPVs is also observed for the two random copolymers LC-PPV and PhS-PPV. Clearly, the symmetric LC-PPV shows a morphology that is dominated by a number of large, structureless aggregates (see Figure 2b). Actually, the aggregation is so strong that reasonable films can only be spin-cast from concentrations significantly below the 3 mg/mL, which is used as standard for all other materials discussed here. On the other hand, the morphology of the unsymmetric PhS-PPV only shows individual chains. In contrast to the unsymmetric homopolymers, no coiled-up conformations are observed.
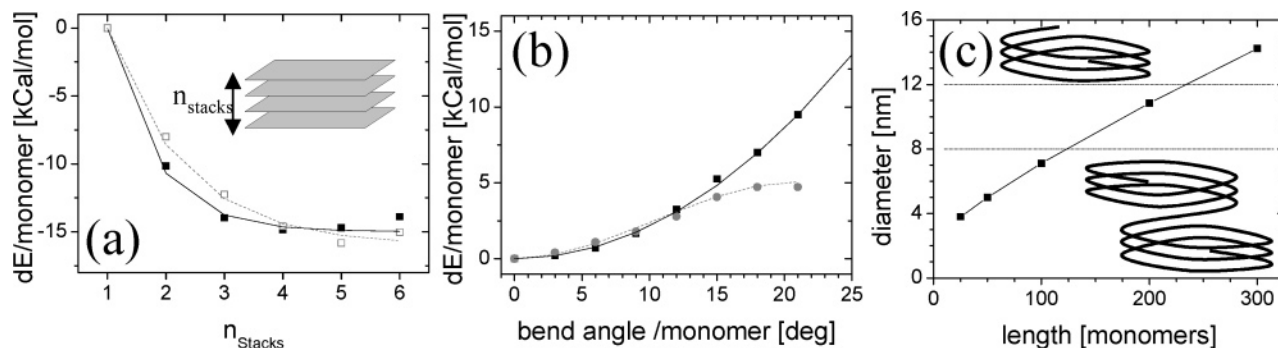
Figure 4. (a) Calculated energy changes per monomer dE of OC_1C_{10}-PPV vs stacking height. The solid (open) symbols are for regular (irregular) stacking (see text). The inset illustrates the stacking, with the polymer chains represented by gray planes. (b) d*E* vs bending angle. Squares (circles) denote planar (free) bending (see text). The lines in (a) and (b) are fits to the data points. (c) Diameter of minimal energy vs length. The horizontal lines indicate the range of experimentally observed diameters. The upper inset is a cartoon of the coiled-up conformation; connected rings, as observed for OC_1C_{10}- and MEH-PPV are formed by a change in the spiraling sense (see lower inset).

Rather, the molecular chains appear to be in a (boiled) spaghetti-like conformation.

From the observations in Figures 1 and 2, it seems safe to conclude that the symmetry of the substitution pattern has a profound influence on the (surface) morphology of spin-cast films. Symmetric substitution causes the chain to adopt a conformation that is, at least over a certain length, straight, which enables the formation of interchain aggregates. Unsymmetric substitution effectively seems to prevent the formation of these interchain aggregates. In a number of cases coiled-up conformations form, which, in our opinion, may be regarded as self- or intrachain aggregates. This issue will be discussed in more detail in the next subsection.

It is tempting to interpret the typical feature size in Figures 1 and 2 as indicative for either the conjugation length, i.e., the typical distance between two conjugational defects, or for the chain length. In the present situation, we cannot tell whether these assignments are correct. The latter assignment requires that the entire chain is arranged on the film surface, which one cannot tell from the images. The former demands a resolution that is sufficient to distinguish individual monomers, i.e., subnanometer-sized features, whereas our resolution is limited to a few nanometers.

We now compare our observations to macroscopic observables. It is commonly accepted that interchain aggregation, or any decrease in the conformational disorder in general, increases the charge carrier mobility.[3,4,17] Therefore, on the basis of the observed morphologies, one expects a larger mobility for the symmetrically substituted PPV than for the unsymmetric ones. This is in perfect agreement with the zero-field mobility (μ_0) data in Table 1. However, no significant differences between the value of γ, which is related to the broadening of the density-of-states,[5,17,18] for the various materials are observed. The field effect mobility, μ_{FET}, shows a similar correlation with the morphology as μ_0. This could be taken as an indication that the morphology at the substrate–polymer interface is comparable to that at the polymer–air interface. However, the values of μ_{FET} shown in Table 1 are mostly obtained on hydrophobicized SiO_2 substrates. Therefore, any claims on morphological similarity between the images shown in the present paper and the morphology at the substrate–polymer interface in actual FETs must be regarded as tentative. For this reason we will not further discuss μ_{FET} values.

The present results also offer a visualization and a confirmation of the morphological differences between various (un)symmetric dialkoxy-PPVs that were invoked by Warman et al. to explain differences in time-resolved microwave conductivity.[19] In ref 19 a larger conductivity is observed for symmetric PPV derivatives, which is attributed to a stronger tendency to aggregate, entirely in line with Figures 1 and 2.

The interpretation of the circular features in the morphology of OC_1C_{10}-PPV as self-aggregates implies that the characteristic signs of aggregation should be visible in photoluminescence (PL) spectra as well, provided that the observed surface morphology is characteristic for a significant part of the entire film. In Figure 3a, the PL spectra of OC_1C_{10}-PPV in solution (symbols) and film (solid line) are shown. The increased spectral weight of the red-shifted shoulder at 621 nm with respect to the main emission peak at 578 nm in the solid state compared to the solution shows that there is indeed a significant amount of (self-)aggregation present in the film. For MEH-PPV, shown in panel b, the spectral weight of the vibronic shoulder at 614 nm is hardly increased in the solid-state spectrum as compared to the spectrum obtained in solution. Also, the shift of the main emission peak, from 563 to 576 nm, is less than for OC_1C_{10}-PPV (561 and 578 nm in solution and film, respectively). Both effects indicate a smaller degree of (self-)aggregation in MEH-PPV than in OC_1C_{10}-PPV, in correspondence with the lesser extent in which the self-aggregates are developed in the former material (see Figure 1a,c).

Further confirmation or rejection of the proposed interpretation of our AFM data may be sought for by comparison with polarization- or time-resolved spectroscopy experiments. However, it was found that these experiments are largely determined by the dynamics of the excited state that are governed by highly localized features, like traps, defects, and impurities, that are beyond the resolution of our AFM imaging.[20]

The morphological differences between MEH- and BisEH-PPV are also reflected in the optical domain. Zheng et al. interpreted differences in fluorescence behavior between MEH- and BisEH-PPV as the result of a more ordered and extended conformation of the BisEH-PPV chains.[21] Our results seem to confirm this interpretation. On the other hand, aggregation of MEH-PPV in pristine films cast from chlorobenzene is observed in a number of optical experiments,[2,11] which is

seemingly in contradiction with the present result. However, these experiments are done on another batch of MEH-PPV, which may differ from the present one in terms of defects (both in nature and occurrence), molecular weight, polydispersity, etc. Moreover, it is virtually impossible to distinguish optically between inter- and intrachain aggregates in films. On basis of our present results, we suggest that the former (latter) are dominant on BisEH-PPV (MEH-PPV). Second, it should be kept in mind that the present images only reflect the morphology in the top layer of the film. Although the observed morphologies seem to be in good qualitative agreement with macroscopic (bulk) observations, the morphology in deeper layers still may differ from that in the top layer.

Finally, our results are consistent with the conclusion of Peeters et al., who found for a series of chiral dialkoxy PPVs that a high degree of unsymmetry in the substitution pattern precludes interchain ordering of the polymer chains.[22]

Molecular Dynamics Simulations. To gain more insight in the nature of the coiled-up conformations that are observed for OC_1C_{10}- and MEH-PPV, molecular dynamics calculations were performed on the former polymer.[23] In our previous work[14] we have shown that OC_1C_{10} macromolecules have a clear tendency to bend, a tendency that is absent in $BisOC_{10}$ macromolecules. Moreover, we have found that, in the absence of conformational defects, the coil is indeed the conformation with the lowest energy in these calculations. The time scales that are accessible in this type of calculations, i.e., up to about 100 ps, are by far too short to observe the spontaneous formation of coils from a straight starting position. Therefore, we here use an indirect method to estimate the preferential coil diameter d of an isolated chain. In general, for a chain of a given number of monomers N, d is determined by two competing effects. Increasing the number of turns increases the amount of $\pi-\pi$ overlap and hence decreases the total energy. On the other hand, decreasing the number of turns decreases the bending-induced stress in the chain, which also decreases the total energy.

In Figure 4a, the energy gain per monomer associated with the stacking of a number of straight macromolecules is plotted.[24] As expected, the energy gain per added macromolecule decreases with increasing number of macromolecules, finally to become zero for $n_{stack} \geq 4$. The shown calculation has been performed for a stack of regioregular macromolecules, all with the OC_{10} side chains pointing to one side (syn conformation). To test the role of regioregularity and orientation of the alkoxy side chains with respect to each other, a number of other stacks were investigated. We found that the associated energy gain was very similar to that shown by the solid symbols. The largest difference in dE was found for a stack of a regioregular macromolecules with the side chains pointing in opposite directions for alternating layers. The result of this stack is shown by the open symbols in Figure 4a.

The energy cost associated with the bending of the conjugated backbone was calculated in two different ways. First, a dimer was built and relaxed, and then the desired bending angle was introduced in each vinylene bond. The resulting dimer was relaxed again, under the condition that the backbone remains planar, while the two outermost atoms of the dimer were kept in place. The energy cost was then obtained by subtrac-

tion of the energies of the straight and bended dimers. The second method was similar in nature, but instead of a single dimer, two stacked 10-mers were used, and the condition of planarity was dropped. Only for large bending angles, the second method, shown by the circles in Figure 4b, gave lower values for dE. This is due to an additional torsion in the backbone, which relaxes the total strain.

Using the fits through the solid squares in Figure 4a,b, it is trivial to calculate the energetically most favorable diameter for an arbitrary N-mer. The result is shown in panel c. Experimentally, it is hard to conceive how a well-dissolved polymer chain with a number of monomer units of the order of 1000 can spiral up to form a single coil. In addition, the optimal diameter of this coil would be unrealistically large (cf. Figure 4c). Therefore, the number N should, in our opinion, be regarded as a persistence length, here to be regarded as the length over which the polymer chain maintains the same spiraling sense.[25] This allows the formation of multiple, connected rings from a single chain as illustrated in the insets of Figure 4c, in agreement with the observations in Figures 1a,c and 5a. Comparison of Figure 4c with the experimentally observed ring diameters in the range of 8−12 nm gives a persistence length of 100−200 monomers. This is in excellent agreement with the lower limit of 100 monomer units found in our previous work[14] from a purely morphological Monte Carlo simulation.

A posteriori we remark that in the experimentally realistic range of persistence lengths and diameters the bending angle per monomer is sufficiently small to ignore the possible effect of torsion in the backbone (cf. panel b). As torsion is likely to alter the stacking energy, its presence would make our approach, which is based on a decoupling between bending and stacking, less valid.

In the calculations shown we ignored the presence of defects in the actual polymer material. The reason for doing so is that the density of the most abundant defect in OC_1C_{10}-PPV, the tolane−bisbenzyl (TBB) defect,[26] is only 1.5−2.2%, which is well below the critical defect density of 5% which is needed to prohibit the formation of ring- or toroid-shaped conformations.[27] Our simulations show that also the presence of a large number of cis defects causes the ring-shaped conformation to collapse into a rodlike one. The impact of the presence of TBB defects on the experimentally observed morphology is addressed in the last subsection.

The Role of Concentration. So far, only films that were cast from solutions with a concentration of 3 mg/mL were shown. Increasing the concentration to 5 mg/mL or decreasing it to 1 mg/mL yielded no observable effects on the morphology for unsymmetric materials. Apparently, the driving force for self-aggregation remains stronger than that for interchain aggregation, even at a concentration of 5 mg/mL. We should repeat that, on the basis of the current results, this statement can only be made for the surface layer of the film. For symmetric PPV derivatives, the situation is quite different, as is illustrated for BisEH-PPV in Figure 5. Here, a clear increase in degree of aggregation is observed in going from 1 to 5 mg/mL. At the lowest concentration, small aggregates with a typical lateral dimension of 20 nm are observed, in both topography and phase images. At 3 mg/mL, the typical size has increased to 50 nm, but some internal structure still
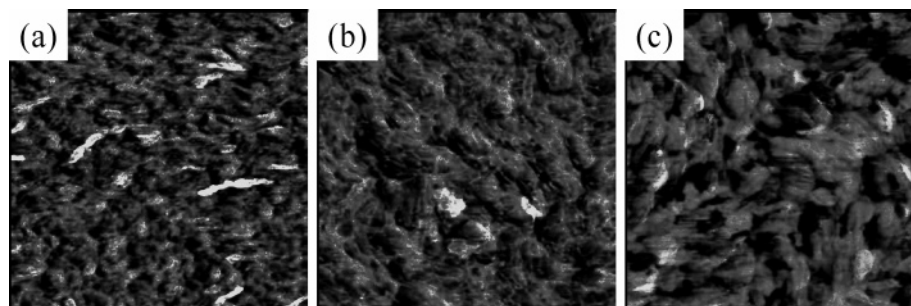
Figure 5. Morphology of BisEH-PPV spin-cast from chlorobenzene with a concentration in solution of (a) 1, (b) 3, and (c) 5 mg/mL. Scan size 500 × 500 nm.
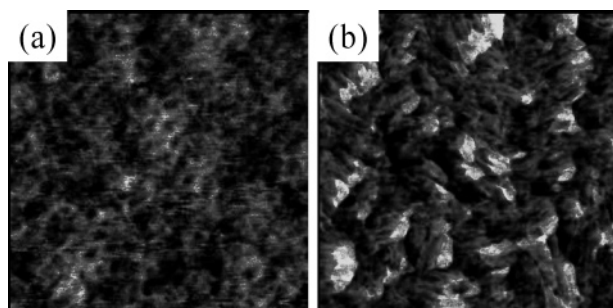

Figure 6. Morphology of (a) MEH-PPV and (b) BisEH-PPV after annealing. Films are spin-cast from chlorobenzene (3 mg/mL). Scan size 200 × 200 nm (a) or 500 × 500 nm (b).

seems to be present in the aggregates. This we attribute to individual chains lying on top of the aggregates. At 5 mg/mL, these features are virtually absent, and quite structureless, 50 nm sized aggregates are observed. These changes in the morphology are accompanied by an increase in the roughness of the film, which is visible in the simultaneously measured height images. Going from 1 to 3 to 5 mg/mL, the rms roughness increases from 0.8 to 2.5 to 3.9 nm.

For $BisOC_{10}$-PPV only 1 and 3 mg/mL solutions were investigated. These yielded results that, though less pronounced, are consistent with those obtained for BisEH-PPV. The same holds for the 1.8 and 5 mg/mL solutions of LC-PPV that were investigated.

The Role of Annealing. Heating of polymer films to temperatures above the glass transition temperature T_g, which is of the order of 75 °C for the materials used here,[28] is well-known to enable a reorganization of the polymer chains into a thermodynamically more favorable conformation. Therefore, one would expect a further development of the intra- and interchain aggregates that are discussed above upon annealing. For MEH- and BisEH-PPV these effects are indeed observed (see Figure 6). Comparison of Figure 6a with panel c of Figure 1 shows that the spiraling self-aggregates have developed further, as reflected by the more pronounced circular features in the former image. Like on OC_1C_{10}-PPV, these have a characteristic diameter of 10 nm. The interchain aggregation that is already present in the pristine films of BisEH-PPV (Figure 5b) is further enhanced in the annealed film (Figure 6b). This, we conclude from the larger number of 50 nm-sized features with a high *relative* brightness in the phase image of the latter film and the accompanying increase in the rms roughness from 2.5 to 3.0 nm. The bright features lack the internal structure that is observed in all similar sized structures in the pristine film, which indicates that a more complete aggregation is achieved by the annealing step. The enhanced brightness of the ag-

gregates in the annealed film, indicating a larger phase shift, can be due to (a combination of) two independent mechanisms. First, it may result from a closer stacking of the polymer chains, which results in an enhanced $\pi-\pi$ overlap and hence in a larger polarizability of the aggregate. Alternatively, it may result from a reorientation of the polymer chains in such a way that an axis of larger polarizability is turned parallel to the surface normal. As the π orbitals are mainly responsible for the observed phase contrast, this would indicate a reorientation from a situation with the b-axis of the chains in the surface plane to a situation with the b-axis perpendicular to the surface plane. An enhanced in-plane orientation of the polymer chain after annealing has been observed by Liu et al. for MEH-PPV,[28] which is consistent with the latter scenario. Moreover, it is entirely consistent with our interpretation of the circular features in Figures 1 and 6 and their enhancement upon annealing, since the proposed conformation implies the in-plane orientation of the polymer chain, i.e., with the b-axis perpendicular to the surface plane.

Annealing of the MEH-PPV film resulted in a red shift of the maximum of the emission spectrum from 576 to 584 nm. Moreover, the vibronic shoulder seems slightly more developed after annealing. In a large number of papers, similar effects in the PL spectra of MEH-PPV are interpreted in terms of enhanced interchain interactions due to stronger aggregation after annealing.[2,11,12,29] However, as was argued above, it is extremely hard to distinguish optically between inter- and intrachain aggregates, and the observed changes in PL could, in our opinion, also be due to enhanced intrachain aggregation. The latter would be in perfect agreement with our morphological observations (cf. Figures 1c and 6a). On the other hand, we still cannot exclude the presence of interchain aggregates deeper in the film.

To explain the optical shift discussed above and a smoothening of topographical AFM images, Schwartz et al. propose a straightening of the polymer strands of MEH-PPV upon annealing.[2] Our results show that, at least in the surface layer, the polymer strands do not straighten to form interchain aggregates but rather coil up to form self-aggregates. To this observation we should add that the large topographic features that were observed in the AFM images of ref 2 are not observed on our films. Actually, no significant topographical changes in terms of roughness or feature size were observed upon annealing our MEH-PPV films.

Not so pronounced results were obtained for the pair OC_1C_{10}- and $BisOC_{10}$-PPV. For the former, no significant changes in the morphology were observed. This can either reflect that the pristine morphology is already quite close to thermodynamic equilibrium, or it may
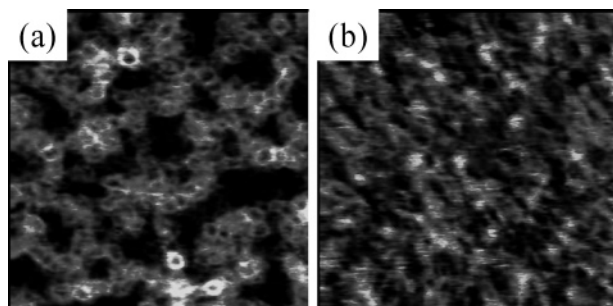
Figure 7. Morphology of OC_1C_{10}-PPV spin-cast from (a) warm *o*-xylene and (b) cyclohexanone. Both films are pristine and had a concentration in solution of 3 mg/mL. Scan size 200 × 200 nm.

Figure 8. Morphology of OC_1C_{10}-PPV synthesized via the sulfoxy route. The film is pristine, and the scan size is 200 × 200 nm.

simply reflect our disability to resolve the relatively small contrast between coils with a different number of turns. The fact that there is only a minimal difference in the PL spectra of the pristine and annealed films of OC_1C_{10}-PPV (cf. the solid and dashed lines in Figure 3a) evidently favors the former interpretation. For $BisOC_{10}$-PPV some reorganization seemed to occur, but no reproducible effects could be observed in the morphology.

As expected, annealing of the already completely aggregated LC-PPV film did not produce any appreciable difference in the degree of aggregation. Annealing the PhS-PPV films did not result in a noticeable change in the topography, which is in perfect correspondence with the absence of any signs of aggregation in the optical spectra of these films.[30] Apparently, the PhS side groups are bulky enough to prevent aggregation.[28,31]

The Role of the Solvent. So far, only films that are spin-cast from chlorobenzene were discussed. Since it is well-known that the film properties and morphology depend strongly on the solvent that is used in the casting process,[2,11,13,32] we investigated two other solvents for two types of OC_1C_{10}-PPV, i.e., synthesized via the Gilch and sulfoxy routes, see also next subsection. As we found virtually identical morphologies for both materials, only those of the Gilch material are shown in Figure 7.

The circular features that are observed in the morphology of OC_1C_{10}-PPV spin-cast from chlorobenzene (CB) (see Figure 1a) are also observed for films cast from warm (60 °C) *o*-xylene. The latter is, like CB, generally regarded as a good solvent for these materials, which means that the polymer is molecularly dissolved. This result is entirely consistent with our observation that only the details of the charge transport depend on the solvent, provided that a good solvent and similar processing parameters are used (see Table 1 and its discussion). Something similar seems to hold for the optical characteristics.[32] From a physical point of view, it is reasonable to expect that films of one and the same material, exhibiting a similar morphology, also have similar properties.

Spin-casting the OC_1C_{10}-PPV film from cyclohexanone (CH), which is regarded as a relatively poor solvent, results in a morphology that is strongly reminiscent of that of PhS-PPV cast from CB (cf. Figures 7b and 2a). Clearly, the coiled-up conformations that are characteristic for the good-solvent films are absent in Figure 7b, which shows that the conformations adopted in solution, i.e., either in the prepared solution or in the
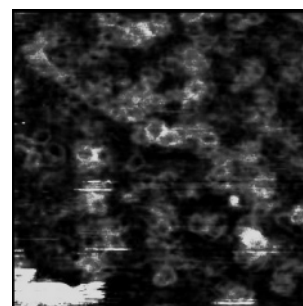
more concentrated wet film during the drying process, are of direct influence on the solid-state morphology.

Finally, it is interesting to note that annealing of CH-cast OC_1C_{10}-PPV films does not result in a significant change in morphology. This illustrates the fact that in the solid state the polymer chains have only a limited amount of freedom to rearrange into a more favorable conformation upon heating above the glass temperature. Apparently the chains are so strongly entangled in their pristine conformations that formation of the energetically more favorable coiled self-aggregates is inhibited.

The Role of the TBB Defect. It was recently found by Inigo et al.[33] that an increased tetrahedral defect density correlates with a lower charge mobility for MEH-PPV. Moreover, Gelinck et al. found, for a series of OC_1C_{10}-PPVs, that the carrier mobility strongly decreases with increasing degree of conjugation breakage.[34] It is logical to expect that conjugation-breaking defects directly hamper the charge transport by acting as hopping barrier, as trapping site, etc. However, one can imagine an indirect effect as well via the morphology. Since structural defects in general affect the mechanical properties of the conjugated backbone, as was discussed in the subsection on MD calculations, the morphology may be different for materials with different defect densities. This in turn may give rise to differences in mobility. As a first step to test this hypothesis, we have studied the morphology of OC_1C_{10}-PPV synthesized via the sulfoxy route. All materials discussed so far were synthesized via the Gilch route.[24] The predominant structural defect in Gilch-OC_1C_{10}-PPV is the tolane−bisbenzyl (TBB) defect, which has a typical occurrence of 1.5−2.2%. This means that 3.0−4.4% of the vinylene bonds are replaced by single and triple bonds. When synthesized via the sulfoxy route, this defect is absent in OC_1C_{10}-PPV.[35]

Comparison of Figure 8 with Figure 1a shows that the absence of the TBB defect does not significantly influence the (surface) morphology of OC_1C_{10}-PPV. This is in agreement with the findings in the MD calculations, where it is argued that the TBB defect density is below the critical density, above which toroid conformations are expected to collapse into rod-shaped conformations. However, because of the different defect contents of the two materials, the similarity in morphology of Gilch- and sulfoxy-OC_1C_{10}-PPV does not imply that the charge carrier mobilities are expected to be identical.

Conclusions

We have investigated the role of the substitution pattern and the influence of preparation conditions on the molecular-scale morphology of PPV derivatives in

spin-cast films. In most cases, it turned out to be very well possible to consistently relate the observed surface morphologies to bulk observables like the charge carrier mobility and PL spectra. This is taken as a strong indication that the measured surface morphology generally may be taken as indicative of the morphology of the bulk. However, extreme care should be taken when general rules about the relation between the observed morphology and macroscopic properties are to be induced from a limited set of observations.

We found that a symmetric substitution pattern strongly promotes interchain aggregation in the surface layer of the film, whereas an unsymmetric pattern in some cases leads to intrachain or self-aggregation. The higher degree of interchain order for symmetric PPVs correlates well with an enhanced carrier mobility on both FET- and LED-type devices. Increasing the polymer concentration in the casting solution leads to more pronounced aggregation for one symmetrically substituted material; for unsymmetric substitution no significant effects are observed. Heating the films above the glass transition temperature is found to enhance both inter- and intrachain aggregation in those cases where thermodynamically more favorable conformations are close to the pristine conformation. This is a direct result of the limited freedom of the polymer chains in the solid state, even if $T > T_g$. For a particular polymer, OC_1C_{10}- or MDMO-PPV, the role of solvent and defect content was investigated in some detail. Changing the solvent to another good (bad) solvent resulted in a similar (different) morphology. Removal of the most abundant conjugation breaking defect did not lead to an observable change in morphology.

References and Notes

(1) Friend, R. H.; Gymer, R. W.; Holmes, A. B.; Burroughes, J. H.; Marks, R. N.; Taliani, C.; Bradley, D. D. C.; Dos Santos, D. A.; Brédas, J. L.; Löglund, M.; Salaneck, W. R. *Nature (London)* **1999**, *397*, 121.
(2) For a recent review see e.g.: Schwartz, B. J. *Annu. Rev. Phys. Chem.* **2003**, *54*, 141.
(3) Martens, H. C. F.; Blom, P. W. M.; Schoo, H. F. M. *Phys. Rev. B* **2000**, *61*, 7489.
(4) Sirringhaus, H.; Brown, P. J.; Friend, R. H.; Nielsen, M. M.; Bechgaard, K.; Langeveld-Voss, B. M.; Spiering, A. J. H.; Janssen, R. A. J.; Meijer, E. W.; Herwig, P.; de Leeuw, D. M. *Nature (London)* **1999**, *401*, 685.
(5) Tanase, C.; Meijer, E. J.; Blom, P. W. M.; de Leeuw, D. M. *Phys. Rev. Lett.* **2003**, *91*, 216601.
(6) Brabec, C. J.; Sariciftci, N. S.; Hummelen, J. C. *Adv. Funct. Mater.* **2001**, *11*, 15. Coakley, K. M.; McGehee, M. D. *Chem. Mater.*, in press. Hoppe, H.; Sariciftci, S. N. *J. Mater. Res.* **2004**, *19*, 1924.
(7) Ho, P. K. H.; Thomas, D. S.; Friend, R. H.; Tessler, N. *Science* **1999**, *285*, 233.
(8) Möller, S.; Perlov, C.; Jackson, W.; Taussig, C.; Forrest, S. *Nature (London)* **2003**, *426*, 166.
(9) Smits, J. H. A.; Meskers, S. C. J.; Janssen, R. A. J.; Marsman, A. W.; de Leeuw, D. M. *Adv. Mater.* **2005**, *17*, 1169.
(10) Cornil, J.; Beljonne, D.; Calbert, J.-P.; Brédas, J.-L. *Adv. Mater.* **2001**, *13*, 1053.
(11) Nguyen, T. Q.; Martini, I. B.; Liu, J.; Schwartz, B. J. *J. Phys. Chem. B* **2000**, *104*, 237.
(12) Lee, T.-W.; Park, O. O. *Adv. Mater.* **2000**, *12*, 801.
(13) Geens, W.; Shaheen, S. E.; Wessling, B.; Brabec, C. J.; Poortmans, J.; Sariciftci, N. S. *Org. Electron.* **2002**, *3*, 105.
(14) Kemerink, M.; van Duren, J. K. J.; Jonkheijm, P.; Pasveer, W. F.; Koenraad, P. M.; Janssen, R. A. J.; Salemink, H. W. M.; Wolter, J. H. *Nano Lett.* **2003**, *3*, 1191.
(15) The lack of discernible topographic features at points where phase contrast is present may due to the fact that the phase signals studied here are usually very weak—a few degrees—and much more sensitive than the topographic signal. In the case of strong interchain aggregation, which gives much larger phase shifts—tens of degrees—this correspondence is present, as expected.
(16) van Breemen, A. J. J. M.; Herwig, P. T.; Chlon, C. H. T.; Sweelssen, J.; H. F. M. Schoo, Mena Benito, M. E.; de Leeuw, D. M.; Tanase, C.; Wildeman, J.; Blom, P. W. M. *Adv. Funct. Mater.,* in press.
(17) Bässler, H. *Phys. Status Solidi* **1993**, *175*, 15.
(18) Blom, P. W. M.; Vissenberg, M. C. J. M. *Mater. Sci. Eng. R* **2000**, *27*, 53.
(19) Warman, J. M.; Gelinck, G. H.; de Haas, M. P. *J. Phys.: Condens. Matter* **2002**, *14*, 9935.
(20) Meskers, S. C. J.; Janssen, R. A. J.; Haverkort, J. E. M.; Wolter, J. H. *Chem. Phys.* **2000**, *260*, 415.
(21) Zheng, M.; Bai, F.; Zhu, D. *Polym. Adv. Technol.* **1999**, *10*, 476.
(22) Peeters, E.; Janssen, R. A. J.; Meijer, E. W. *Synth. Met.* **1999**, *102*, 1105.
(23) HyperChem Pro V6.0.1 Molecular Modeling System, using MM+ force fields. Hypercube, Inc., 2000.
(24) Each macromolecule consists of 10 monomers. The total energy of the macromolecule was found to be linear in the number of monomers for $N > 5$.
(25) The persistence length used here may be significantly larger than the conventional persistence length, which is the average length over which the chain has the appearance of a rigid segment. See e.g.: Kleman, M.; Lavrentovich, O. D. In *Soft Matter Physics: An Introduction*; Springer: New York, 2003; Chapter 15.
(26) Becker, H.; Spreitzer, H.; Kreuder, W.; Kluge, E.; Schenk, H.; Parker, I.; Cao, Y. *Adv. Mater.* **2000**, *12*, 42.
(27) Hu, D.; Yu, J.; Wong, K.; Bagchi, B.; Rossky, P. J.; Barbara, P. F. *Nature (London)* **2000**, *405*, 1030.
(28) Liu, J.; Guo, T.-F.; Yang, Y. *J. Appl. Phys.* **2002**, *91*, 1595.
(29) Tan, C. H.; Inigo, A. R.; Hsu, J.-H.; Fann, W.; Wei, P. K. *J. Phys. Chem. Solids* **2001**, *61*, 1643.
(30) Schoo, H. F. M.; Demandt, R.; Liedenbaum, C. T. H. F.; Wijnberg, H.; ten Hoeve, W.; Spoelstra, K. J. International Patent no. WO 99/21936, 1999.
(31) Gettinger, C. L.; Heeger, A. J.; Drake, J. M.; Pine, D. J. *J. Chem. Phys.* **1994**, *101*, 1673.
(32) Inigo, A. R.; Chiu, H.-C.; Fann, W.; Huang, Y.-S.; Jeng, U.-S.; Lin, T.-L.; Hsu, C.-H.; Peng, K.-Y.; Chen, S.-A. *Phys. Rev. B* **2004**, *69*, 075201.
(33) Inigo, A. R.; Chiu, H.-C.; Fann, W.; Huang, Y.-S.; Jeng, U.-S.; Hsu, C.-H.; Peng, K.-Y.; Chen, S.-A. *Synth. Met.* **2003**, *139*, 581.
(34) Gelinck, G. H. Excitons and polarons in luminescent conjugated polymers: a flash-photolysis and pulse-radiolysis study. Ph.D. Thesis, Delft University, The Netherlands, 1998, ISBN 90-407-1787-7; Chapter 6.
(35) Roex, H.; Adriaensens, P.; Vanderzande, D.; Gelan, J. *Macromolecules* **2003**, *36*, 5613.
(36) Spreitzer, H.; Kreuder, W.; Becker, H.; Schoo, H.; Demandt, R. PCT Patent Application WO 98 27 136, 1996.
(37) van Breemen, A. J. J. M.; Issaris, A. C. J.; de Kok, M. M.; Van Der Borght, M. J. A. N.; Adriaensens, P. J.; Gelan, J. M. J. V.; Vanderzande, D. J. M. *Macromolecules* **1999**, *32*, 5728.
(38) L Lutsen, Adriaensens, P.; Becker, H.; van Breemen, A. J.; Vanderzande, D.; Gelan, J. *Macromolecules* **1999**, *32*, 6517.
(39) It should be noted that mobility measurements on space charge limited hole-only devices of MDMO-PPV, spin-cast from chlorobenzene, gave similar hole mobilities as reported in the literature where mostly toluene was used as casting solvent. Blom, P. W. M., private communication.
(40) Campbell, I. H.; Smith, D. L. In *Solid State Physics*; Academic Press: San Diego, 2001; Vol. 55, p 1.
(41) Roichman, Y.; Tessler, N. *Appl. Phys. Lett.* **2002**, *80*, 151.
(42) Blom, P. W. M.; Schoo, H. F. M.; Matters, M. *Appl. Phys. Lett.* **1998**, *73*, 3914.
(43) The LED mobility for the batch PhS-PPV used in this work was measured in the group of Prof. P. W. M. Blom at Groningen University and gave somewhat lower values as reported earlier for another batch in ref 40.

(44) The mobility for BisEH-PPV was measured on space charge limited hole-only devices at room temperature by V. D. Mihailetchi and C. Tanase in the group of Prof. P. W. M. Blom at Groningen University. Hole-only devices were prepared with the configuration glass/ITO/PEDOT:PSS/BisEH-PPV/Au, spin-casting BisEH-PPV from either *o*-dichlorobenzene ($\mu_h = 5 \times 10^{-5}$ cm²/(V s)) or toluene ($\mu_h = 1 \times 10^{-5}$ cm²/(V s)).

(45) The mobility for LC-PPV was measured on space charge limited hole-only devices at room temperature by C. Tanase in the group of Prof. P. W. M. Blom at Groningen University. Hole-only devices were prepared with the configuration glass/ITO/PEDOT:PSS/LC-PPV/Au.